Final Draft
of the original manuscript:

Pyczak, F.; Neumeier, S.; Goeken, M.:
Influence of lattice misfit on the internal stress and strain states before and after creep investigated in rhenium and ruthenium containing nickel-base superalloys
In: Materials Science and Engineering A (2009) Elsevier

DOI: 10.1016/j.msea.2008.08.052

Influence of lattice misfit on the internal stress and strain states before and after creep investigated in rhenium and ruthenium containing nickel-base superalloys

Florian Pyczak[1], Steffen Neumeier*[2], Mathias Göken[2]

[1]Institute for Materials Research, GKSS Research Centre Geesthacht, Geesthacht 21502, Germany

[2]Department of Materials Science & Engineering, Institute I, University Erlangen-Nürnberg, Erlangen 91058, Germany

Abstract

The microstructure of nickel-base superalloys changes significantly during creep. The strengthening γ′-precipitates coarsen directionally and dislocation networks develop at the interfaces between γ′-precipitates and γ-matrix. Coherency stresses due to the lattice misfit between γ and γ′ phase act as the driving force for these microstructural changes.

The measurement of the lattice constant of the γ-matrix and γ′-phase by X-ray diffraction before and after creep experiments allows to see the changes of internal stress and strain states during creep. In this work three experimental alloys with systematically varied amounts of lattice misfit were studied. It was found that the separation of X-ray peaks of γ and γ′ after creep is directly dependent on the amount of lattice misfit. Also the distortion of the lattice, visible in the broadening of the respective rocking curves, was measured and found to be dependent on the lattice misfit as long as the γ/γ′-interfaces stay coherent. The lattice misfit is

directly influenced by the alloy composition. Rhenium and ruthenium decrease the lattice misfit and modify the coherency stresses between γ- and γ′-phase, accordingly.

* Corresponding author; Tel.: 0049-9131-85-27478; Fax.: 0049-9131-85-27504;
e-mail: steffen.neumeier@ww.uni-erlangen.de

Keywords: Superalloys, X-Ray-diffraction, Lattice misfit, Creep, Internal stress

1. Introduction

The presence of up to 70 % of the ordered γ′-precipitate phase contributes to significant strengthening in nickel-base superalloys [1-3]. Initially the γ′-particles form a coherent interface with the face centered cubic nickel solid solution γ-matrix and often possess a cubic shape [4]. Due to slight differences in lattice constants of both phases, γ and γ′, a lattice misfit exists. With increasing temperature the misfit changes as the lattice constant of the γ-matrix increases more strongly than the lattice constant of the γ′-precipitates. During creep deformation especially in the low stress high temperature regime interfacial dislocation networks develop at the γ/γ′-interfaces [5-7]. The γ′-precipitates coarsen directionally either parallel or perpendicular to the external stress axis. The orientation of the directional coarsening is determined by the sign of the lattice misfit between γ- and γ′-phase, as it is caused by a combined effect of the externally applied stress and the coherency stresses between γ and γ′. In later stages of creep the dislocations stored in the networks recover either by cutting γ′-precipitates or by climbing over γ′-precipitates [8]. As the γ′-phase contributes strongly to the creep strength of nickel-base superalloys, the directional coarsening of this phase, the γ/γ′-lattice misfit and the interfacial dislocation networks are of utmost interest.

It is well known that the lattice misfit of nickel-base superalloys is strongly influenced by the alloy composition [9-11]. A number of alloying elements, which are added in the 2nd, 3rd and

4th generation nickel base superalloys, namely rhenium and ruthenium, increase the amount of lattice misfit as they are known to partition preferentially to the γ-matrix. Nanoindentation experiments have shown that rhenium strengthens the γ-matrix phase [12]. Ruthenium on the other hand increases the hardness of the γ′-phase, due to its influence on the partitioning behavior of other alloying elements [13]. Alloys developed by the group of Harada possess a large lattice misfit and show excellent high temperature creep properties [14, 15]. In these alloys dense dislocation networks are found at γ/γ′-interfaces after creep deformation in the low stress and high temperature regime.

Different methods exist to measure lattice misfit and/or lattice constants such as convergent beam electron diffraction (CBED) (e.g. [16-19]), evaluation of interfacial dislocation networks [20, 21], X-ray diffraction (e.g. [22-25]) and neutron diffraction (e.g. [26-28]). Diffraction methods are easily employed and yield not only information about the lattice constants and lattice misfit but also about the lattice distortion. For these reasons X-ray diffraction was frequently used in the past to investigate nickel-base superalloys. The majority of investigations up to now were performed on commercial alloys [23-25, 29]. In these studies phenomena such as the influence of different applied stresses on the change of internal stress and strain states during creep were investigated intensively. In the present work the lattice misfit and the resulting strain and stress states are investigated in three experimental alloys with varying rhenium and ruthenium content before and after creep deformation. This is to the knowledge of the authors the first experimental investigation on alloys with systematically varied lattice misfit by respective additions of rhenium and ruthenium.

2. Experimental

Three experimental alloys (Alloy 0, Alloy Re and Alloy ReRu) with similar alloy composition except the addition of 3 wt.% rhenium or 3 wt.% of rhenium and ruthenium with a directionally solidified (DS) microstructure were cast in a laboratory scale Bridgman unit. The alloy compositions are given in Table 1. The alloys were solution heat treated and subsequently aged for 4 h at 1100 °C and 24 h at 850 °C to produce γ′-precipitates with diameters between 220 nm and 360 nm. The microstructures of the fully heat treated states are shown in Fig. 1. Local enrichments of some alloying elements in the cast structure (especially rhenium) were homogenized during sufficiently long holding times during solution heat treatment

Specimens for creep tests with a diameter of 5 mm and a length of 7.5 mm parallel to the solidification direction were machined from the fully heat treated alloys by means of spark erosion. Compression creep tests were performed in air using an applied stress of 137 MPa at a temperature of 1100 °C. The external stress axis lies parallel to the common [001] orientation of the elongated grains. Samples for X-ray diffraction measurements were prepared by cutting the creep specimens perpendicular to the stress axis allowing to record {002} X-ray peaks (i.e. diffracting at lattice planes perpendicular to the external stress axis).

The X-ray diffraction measurements were done at room temperature with a double crystal diffractometer with monchromized copper $K_{\alpha 1}$ X-rays. By using a setup first proposed by Wilkens and Eckert [30], the instrumental peak broadening was eliminated. Owing to the high angular resolution of the setup, lattice constants were determined with an error in the order of $2x10^{-5}$ nm. All X-ray peaks were recorded as ω-2Θ-scans rotating the specimen in steps of 0.25° around the ω-axis. Details are described in [23]. The {002} peaks at the different angles ω are composed of the {002} sub-peaks of the γ-matrix and the γ′-precipitate phase, respectively. Due to the fact that the differences in lattice constant between the two phases are very small, the two sub-peaks of the phases γ and γ′ normally overlap. To extract the sub-

peaks for the γ- and γ′-phase from the measured integral peak the software XPLOT [31] was used. Either two sub-peaks for the γ- and the γ′-phase were fitted if their sum satisfactorily resembled the integral peak or in the fully heat treated state of Alloy ReRu up to three sub-peaks were used to represent the contributions of the γ′- and the γ-phases of the two different kinds of matrix channels perpendicular and parallel to the specimen surface. A combination of Gaussian and Lorentzian peak shapes was used for the fit. From the lattice constants of the γ- and γ′-sub-peaks the lattice misfit was derived as

$$\delta = \frac{2(a_{\gamma'} - a_{\gamma})}{a_{\gamma'} + a_{\gamma}}.$$

Here $a_{\gamma'}$ is the lattice constant of the γ′- and a_{γ} of the γ-phase, respectively. For the standard heat treated state of Alloy ReRu the lattice misfit given in this work is an average misfit [32] as it was necessary to deconvolute the overall profile in a γ′- and two separate γ-sub-peaks to achieve an acceptable fit,. The error of lattice constant measurement, given above, results in an error in misfit determination of about 0.01 %. All misfits given in this work are directly derived from the X-ray profiles and represent the constrained misfit in the case of the standard heat-treated states with coherent γ/γ′-interfaces and a combination of the constrained misfit and the strain contributions from the interfacial dislocation networks in the specimens investigated after creep. In order to derive lattice constants and misfits in the manner described above, sum profiles adding up the X-ray intensity of all profiles of the ω-2Θ-scan recorded at different angles ω were analyzed.

To gain information about the angular distortion in the two phases, γ and γ′, rocking curves were processed from the intensity distribution in the ω-2Θ-scan at the diffraction angles of γ- and γ′-phases, respectively (Fig. 2). In the case of some ω-2Θ-scans, more than one peak was present in these rocking curves resulting from contributions from more than one dendrite. In

such cases the contributions of the single dendrites to the rocking curve were derived by fitting the peaks with XPLOT [31].

3. Results and Discussion

After standard heat treatment the three alloys show different constrained lattice misfits at room temperature varying between 0.11 % for Alloy 0, near zero for Alloy Re and a negative lattice misfit of -0.23 % for Alloy ReRu. The lattice parameters of the phases γ and γ′ are given in table 1. The lattice constant of the γ′-phase in Alloy 0 and Alloy Re is only slightly different while the lattice constant of the γ-phase is larger in Alloy Re. This result is easily understandable, as the only difference in alloy composition is the addition of 3 wt.% of rhenium, which is known to partition preferentially to the γ-matrix and accordingly change it's lattice parameter [11]. In Alloy ReRu, the lattice constant of the γ-phase is further increased compared to Alloy Re, while the lattice constant of the γ′-phase is also slightly higher. This is most probably caused by the addition of ruthenium, which increases the lattice constant of γ significantly but also increases the lattice constant of γ′ slightly. The tendency of ruthenium to partition to the γ-phase is not as pronounced as for rhenium. A second effect is probably the reverse partitioning of rhenium, which is reported for some alloys in the presence of ruthenium [33-35]. This would slightly lower the rhenium content in the γ matrix and increase it in the γ′ phase with corresponding effects on the lattice constants.

The width of the ω-profile (rocking curve) reflects the angular distortion of the lattice. In the absence of interfacial dislocation networks it should be governed by three factors: The amount of lattice misfit, the stiffness of the two phases and the width of the matrix channels. A large amount of lattice misfit requires a high angular distortion of both phases for coherent interfaces. Nevertheless, the elastically stiffer phase gets less distorted. Results of

nanoindentation measurements, published by Göken et al. [36], found that the γ′-phase is elastically stiffer than the γ-phase. In contradiction Siebörger et al. [37] measured single phases reassembling the composition of the γ- and γ′-phase of CMSX-4 by resonance method and here the matrix phase was elastically stiffer for temperatures below 1000 °C. Additionally, if the matrix channels are narrow, angular distortion may not be pronounced but the lattice planes of the γ-phase over the whole width of the matrix channel could be strained to reach a lattice constant near that of the γ′-phase. Additionally the presence of slightly misoriented volumes in the specimens which results in multiple peaks at different angles ω should be also considered. It cannot be ruled out fully that the mosaic structure also alters the width of the single peaks in the ω-direction. In Fig. 3 the full width at half maximum of the rocking curves for the standard heat-treated states of Alloy 0, Alloy Re and Alloy ReRu is plotted versus the amount of constrained lattice misfit. The differences in the widths of the rocking curves correspond to the change in the amount of lattice misfit resulting in lower distortion in the alloy with nearly zero misfit (Alloy Re) compared to the two alloys with either positive (Alloy 0) or negative lattice misfit (Alloy ReRu). Also the γ-matrix is always slightly more distorted than the γ′-phase. This would correspond with the results of Göken et al. [36] stating that the γ′-phase is elastically stiffer than the γ-matrix.

In Fig 4 the strain rate is plotted versus the plastic strain during creep for each alloy. The creep resistance of the alloys improves with increasing amount of rhenium and ruthenium with a minimum creep rate of 10^{-4} s^{-1} for Alloy 0, $6x10^{-7}$ s^{-1} for Alloy Re and $2x10^{-7}$ s^{-1} for Alloy ReRu.

Fig. 5 shows X-ray profiles of the crept specimens (full symbols) in combination with the profiles measured for the state after the standard heat-treatment (open symbols). While the profile of Alloy 0 after creep deformation resembles the shape prior to creep, significant changes in profile shape are found in Alloy Re and Alloy ReRu. The separation of the sub-

profiles, which is especially visible for Alloy ReRu, is known to be caused by the dislocation networks which form during creep deformation [23]. In Fig. 6 the lattice misfit is plotted versus the sum of Re and Ru contents. The (constrained) lattice misfit in the standard heat-treated specimens is directly related to the alloy composition as already described above. After creep deformation the lattice misfit in Alloy 0 is almost the same as in the standard-heat treated state while the lattice misfit changes significantly in Alloy Re and Alloy ReRu. During creep in the high temperature low stress regime as investigated in this study plastic deformation is caused by dislocation loops moving in the γ-channels leaving dislocation segments at the γ/γ′-interface, which form interfacial dislocation networks. It is suggested that this mechanism is active up to the point when the back stress of the dislocations stored in the networks makes it impossible for new dislocations to enter the matrix channel [38, 39]. Then the recovery of dislocations already stored in the matrix channels is necessary before dislocations can enter the channel. This recovery can either happen by cutting of γ′-precipitates or by climbing of dislocations around γ′-particles. Which of the two processes of recovery is encountered and what density of dislocations in the interfacial networks is reached before recovery sets in, is dependent on different factors. In the case of precipitates which do not coarsen directionally, like those in Alloy 0 (Fig. 7), the process of climb is probably more attractive compared to cutting a hard ordered intermetallic phase. In Alloy Re and Alloy ReRu with their directionally coarsened microstructure recovery processes by cutting of γ′-precipitates should happen.

The point, where recovery of the dislocations stored at the γ/γ′-interface is necessary before new dislocations can enter the matrix channel is determined by the amount of coherency stresses in the channel [21, 39]. These coherency stresses themselves are higher if the amount of constrained lattice misfit before deformation is higher (i.e. for the fully coherent γ/γ′-interface). As long as the incorporation of new dislocations into the interfacial networks

further relaxes the coherency stresses this process should be favorable. In the later stages of creep deformation, not only the coherency stresses are relaxed, but stresses in the opposite direction are introduced by interfacial dislocations as has been calculated by Müller et al. [40]. Experimentally this was also shown by Lu et al. by means of CBED measurements [19]. At a certain point the externally applied stress is not high enough to overcome the increasing back stress of the interfacial networks. Starting from this point, recovery of interfacial dislocations is necessary, before new dislocations can enter the matrix channel. Hence, the dislocation networks at the γ/γ′-interfaces should reach a certain equilibrium density [29], which increases with the magnitude of the coherency stresses at creep temperature resulting in an accordingly high separation of X-ray peaks measurable in crept specimens. Dislocation networks at γ/γ′-interfaces were found in Alloy Re and Alloy ReRu after creep. An example for Alloy Re is shown in Fig. 8. Theoretical work by Probst-Hein et al. [39] supports this view. The dependence of the separation of X-ray peaks after creep on the constrained lattice misfit prior to creep found for the alloys under investigation in this work is in accordance with this explanation. In addition, the fact that Harada and coworkers [14, 15] report, that an increasing density of interfacial dislocation networks is found after creep deformation for alloys with high lattice misfit in the initial state supports the present results.

The lattice misfit measured in creep deformed specimens is also dependent on the externally applied stress (e.g. [23]) and the width of the γ-matrix channels [29]. As all three alloys investigated in this work were deformed under the same applied external stress, the differences in the measured lattice misfit after creep cannot be related to different levels of externally applied stress. Furthermore, the channel widths in the creep deformed specimens of Alloy 0, Alloy Re and Alloy ReRu are in the same range of 405 to 455 nm.

Hence in this work the coherency stresses caused by the constrained lattice misfit seem to be the dominating factor controlling the equilibrium density of dislocation networks built during

creep. As the constrained lattice misfit depends on the alloy composition, the alloying elements rhenium and ruthenium influence the density of interfacial dislocations by directly influencing the constrained lattice misfit.

The full widths at half maximum of the rocking curves of the crept specimens of Alloy 0, Alloy Re and Alloy ReRu, which are plotted in Fig. 9, show no clear dependence on the constrained lattice misfit. Interestingly, the width of the rocking curve for the crept specimen of Alloy 0 is almost equal to that of the standard heat-treated state. This is probably due to the fact that the dislocation networks are not well developed in Alloy 0. Therefore the strains at the γ/γ′-interfaces keep the same as in the standard heat-treated state. The direct dependence of the width of the rocking curves on the lattice misfit is lost for the Alloy Re and Alloy ReRu as dislocation networks at the γ/γ′-interfaces have formed.

4. Conclusion

The lattice misfit and internal strain states were investigated by X-ray diffraction in three experimental nickel-base superalloys with systematically varied alloy composition in standard heat treated condition and after creep:

- The addition of rhenium increases mainly the lattice constant of γ with respective effect on the lattice misfit. Alloying ruthenium to a rhenium containing alloy increases the lattice constant of γ further but also increases the lattice constant of the γ′-phase to a lesser extent. This is in accordance with the partitioning behavior of rhenium and ruthenium between γ- and γ′-phase as known from literature.
- While the γ/γ′-interfaces are coherent, the width of the rocking curves of the γ- and γ′-phase are directly dependent on the (constrained) lattice misfit of the alloys. An influence of other parameters as width of γ-channels or different elastic properties of the phases γ

and γ′ was not clearly found. This dependence is lost in the crept specimens when dislocation networks form at the interfaces.

- The sub-peaks of the γ- and γ′-phase were the more separated in the crept specimens the higher the constrained lattice misfit of the respective alloy was. This was assumed to be caused by a higher maximum density of dislocations in the interfacial networks reached before recovery processes begin.

Acknowledgement

The work presented in this paper was financially supported by the German Science Foundation (DFG) in the frame of DFG graduate school 1229. The authors thank the Institute of Science and Technology of Metals of the University Erlangen-Nürnberg for providing access to their Bridgman casting unit.

References

[1] C. Carry, J.L. Strudel, Acta Metall. 26 (1978) 859-870.

[2] M.V. Nathal, J.O. Diaz, R.V. Miner, Proc. MRS Symp., Vol. 133 (1989) 269-274.

[3] H. Rouault-Rogez, M. Dupeux, M. Ignat, Acta Metall. Mat. 42 (1994) 3137-3148.

[4] M. Doi, T. Miyazaki, T. Wakatsuki, Mater. Sci. Eng. 67 (1984) 247-253.

[5] A. Lasalmonie, J.L. Strudel, Phil. Mag. 32 (1975) 937-949.

[6] G.B. Olson, C. Morris, Acta Metall. 27 (1979) 1907-1918.

[7] A.K. Singh, N. Louat, K. Sadananda, Metall. Trans. 19A (1988) 2965-2973.

[8] R. Srinivasan, G.F. Eggeler, M.J. Mills, Acta Mater. 48 (2000) 4867-4878.

[9] M. Fährmann, P. Fratzl, O. Paris, E. Fährmann, W.C. Johnson, Acta Metall. Mater. 43 (1995) 1007-1022.

[10] A. Epishin, U. Brückner, P.D. Portella, T. Link, Scripta Mater. 48 (2003) 455-459.

[11] F. Pyczak, B. Devrient, H. Mughrabi, Proc. Tenth Int. Symposium on Superalloys (2004) 827-836.

[12] K. Durst, M. Göken, Mater. Sc. Eng. A387-389 (2004) 312-316.

[13] S. Neumeier, F. Pyczak, M. Göken, *to be published*

[14] Y. Koizumi, T. Kobayashi, T. Yokokawa, J. Zjang, M. Osawa, H. Harada, Y. Aoki, M. Arai, Proc. Tenth Int. Symposium on Superalloys (2004) 35-43.

[15] J.X. Zhang, J.C. Wang, H. Harada, Y. Koizumi, Acta Mater. 53 (2005) 4623-4633.

[16] R.C. Ecob, R.A. Ricks, A.J. Porter, Scripta Metall. 16 (1982) 1085-1090.

[17] H.J. Maier, R.R. Keller, H. Renner, H. Mughrabi, A. Preston, Phil. Mag. A74 (1996) 23-43.

[18] R. Völkl, U. Glatzel, M. Feller-Kniepmeier, Acta Mater. 46 (1998) 4395-4404.

[19] Z. Lu, F. Pyczak, H. Biermann, H. Mughrabi, Phil. Mag. A82 (2002) 1219-1234.

[20] R.R. Keller, H.J. Maier, H. Mughrabi, Scripta Metall. Mater. 28 (1993) 23-28.

[21] G. Scheunemann-Frerker, L. Müller, M. Feller-Kniepmeier, Phil. Mag. A68 (1993) 193-208.

[22] D.F. Lahrmann, R.D. Field, R. Darolia, H.L. Fraser, Acta Metall. 36 (1988) 1309-1320.

[23] H.-A. Kuhn, H. Biermann, T. Ungár, H. Mughrabi, Acta Metall. Mater. 39 (1991) 2783-2794.

[24] U. Brückner, A. Epishin, T. Link, K. Dressel, Mater. Sc. Eng. A247 (1998) 23-31.

[25] B. von Großmann, H. Biermann, U. Tetzlaff, F. Pyczak, H. Mughrabi, Scripta Mater. 43 (2000) 859-864.

[26] D. Bellet, P. Bastie, Phil. Mag. 64 (1991) 135-141.

[27] U. Glatzel, A. Müller, Scripta Met. Mat. 31 (1994) 285-290.

[28] U. Glatzel, Scripta Mat. 31 (1994) 291-296.

[29] T. Link, A. Epishin, U. Brückner, P. Portella, Acta Mater. 48 (2000) 1981-1994.

[30] M. Wilkens, K. Eckert, Z. Naturf. 19 (1964) 459.

[31] http://www.esrf.eu/computing/scientific/xop2.1/

[32] F. Diologent, P. Caron, T. d'Almeida, S. Chambreland, A. Jacques, P. Bastie, Int. J. Mat. Res. 97 (2006)

[33] K.S. O'Hara, W.S. Walston, E.W. Ross, R. Darolia, US Patent No. 5,482,789, General Electric Company, Cincinnati, OH and Lynn, MA, 1996.

[34] A.P. Ofori, C.J. Humphreys, S. Tin, C.N. Jones, Proc. Tenth Int. Symposium on Superalloys (2004) 787-793.

[35] L.J. Carroll, Q. Feng, J.F. Mansfield, T.M. Pollock, Met. Mat. Trans. 37A (2006) 2927-2938.

[36] M. Göken, M. Kempf, Acta Mater. 47 (1999) 1043-1052.

[37] D. Sieborger, H. Knake, U. Glatzel, Mater. Sc. Eng. A298 (2001) 26-33.

[38] C. Mayr, G. Eggeler, A. Dlouhy, Mater. Sc. Eng. A207 (1996) 51-63.

[39] M. Probst-Hein, A. Dlouhy, G. Eggeler, Acta Mater. 47 (1999) 2497-2510.

[40] L. Müller, U. Glatzel, M. Feller-Kniepmeier, Acta Met. Mat. 41 (1993) 3401-3411.

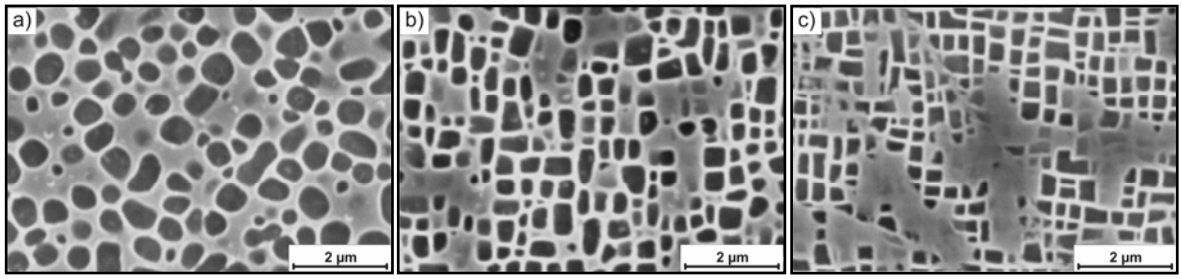

Fig. 1: Microstructure of a) Alloy 0, b) Alloy Re and c) Alloy ReRu in the standard heat-treated state

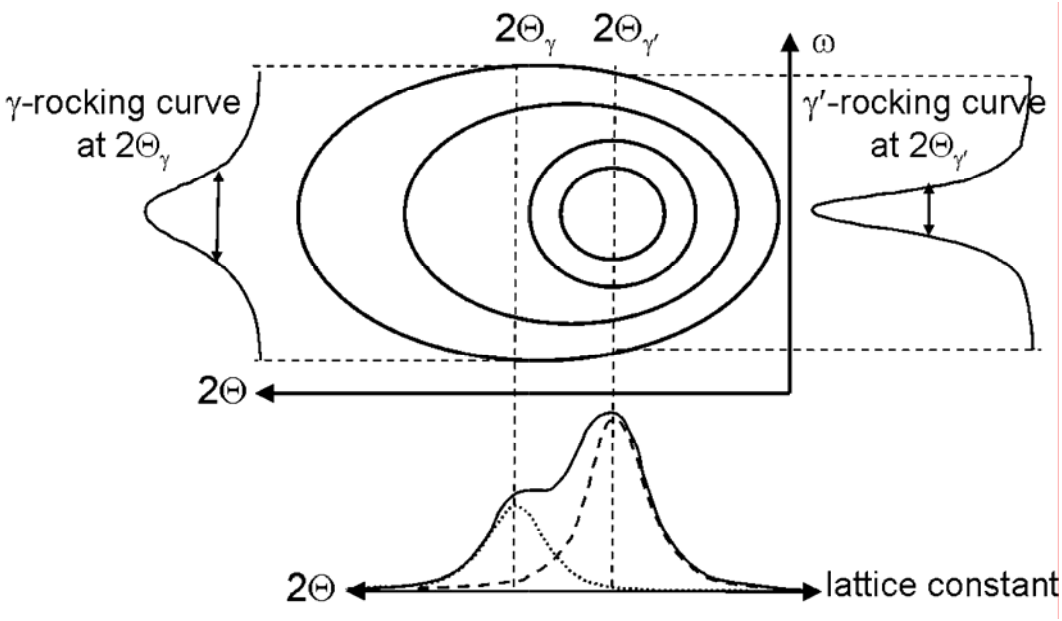

Fig. 2: Scheme how the rocking curves for γ- and γ′-phase, respectively, were derived from the ω-2Θ-scan

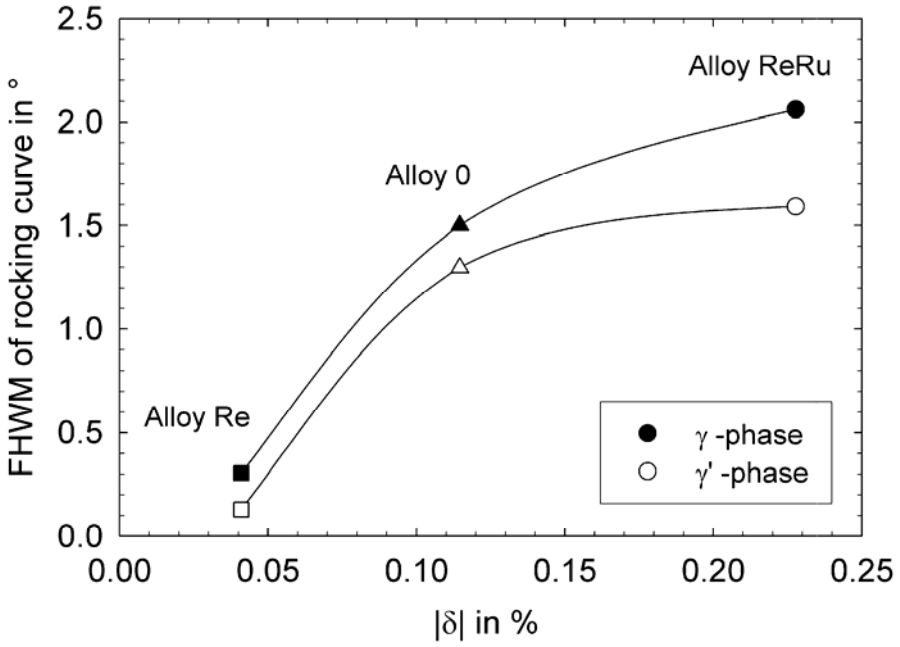

Fig. 3: Change of full width at half maximum of the rocking curves (ω-profiles) of the γ-phase (filled symbols) and γ′-phase (open symbols) of the investigated alloys in the standard heat-treated state as function of misfit δ

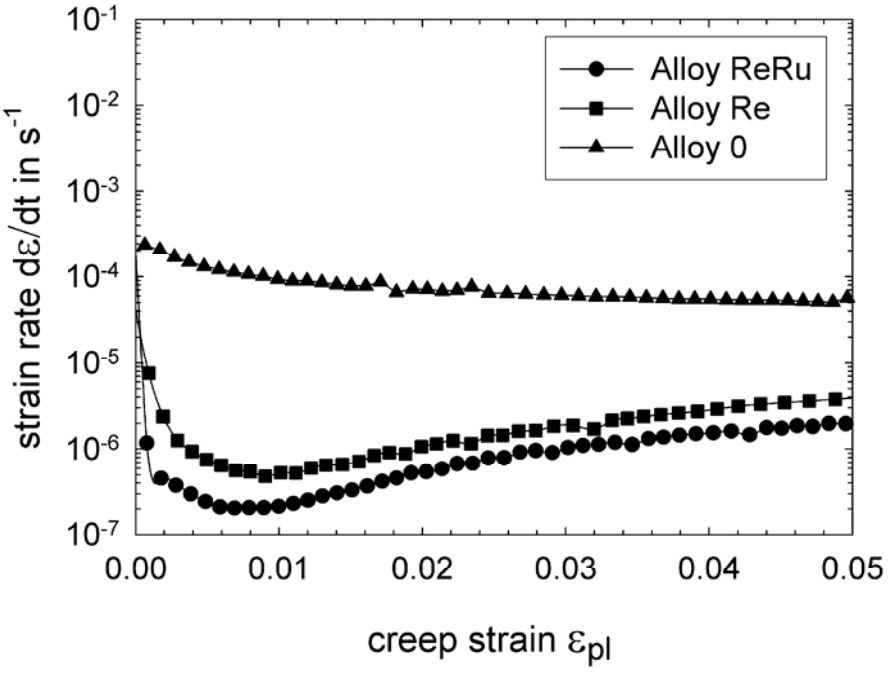

Fig. 4: Strain rate versus plastic strain for the alloys investigated in the present work during creep in compression with an applied load of 137 MPa at a temperature of 1100 °C

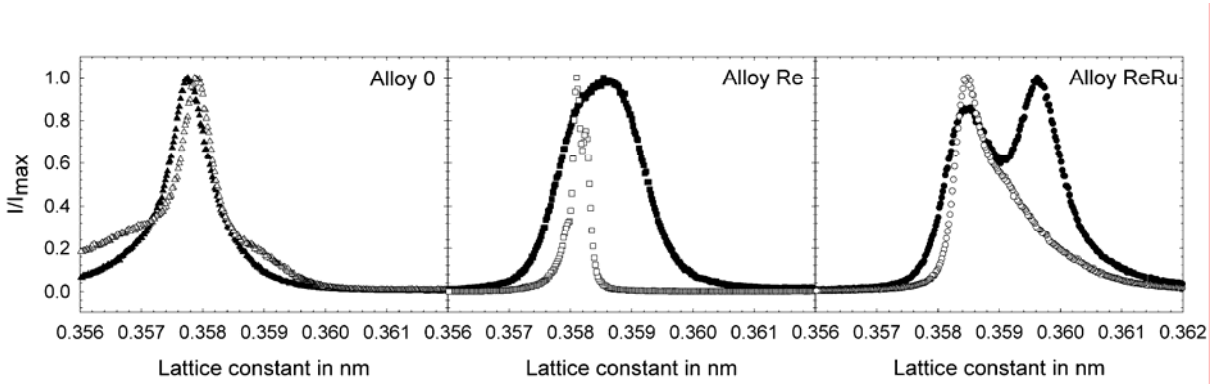

Fig. 5: X-ray profiles of a) Alloy 0, b) Alloy Re and c) Alloy ReRu; open symbols show profile of standard heat-treated specimen and closed symbols for crept specimens

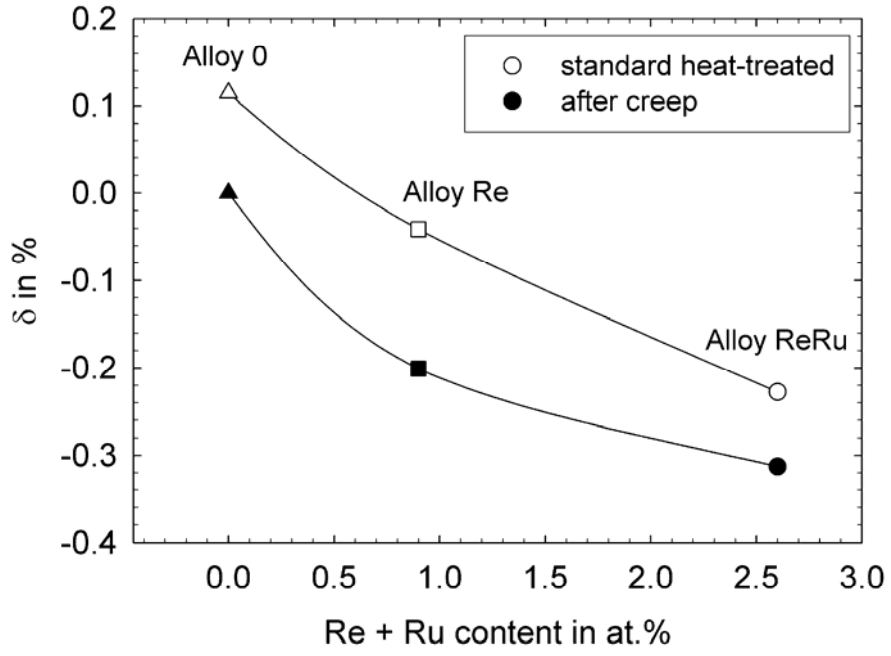

Fig. 6: Dependance of the lattice misfit measured in the standard heat-treated state (open symbols) and subsequent to creep (filled symbols) on rhenium and ruthenium content

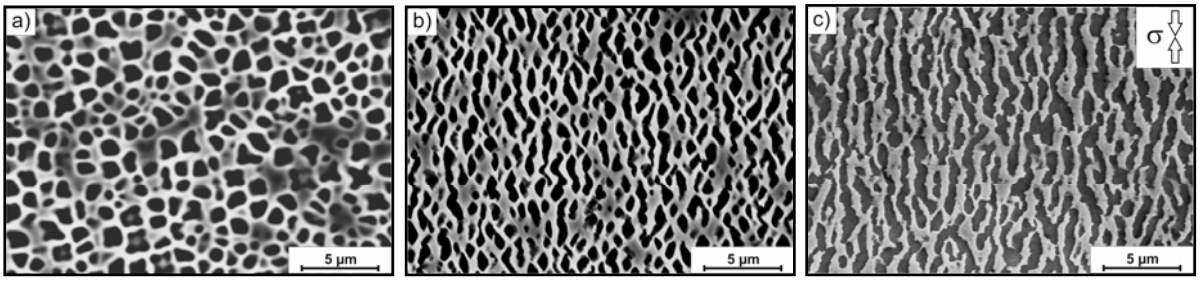

Fig. 7: Microstructure of a) Alloy 0, b) Alloy Re and c) Alloy ReRu in the crept state after a creep time of 0.28 h, 14 h and 28 h, respectively

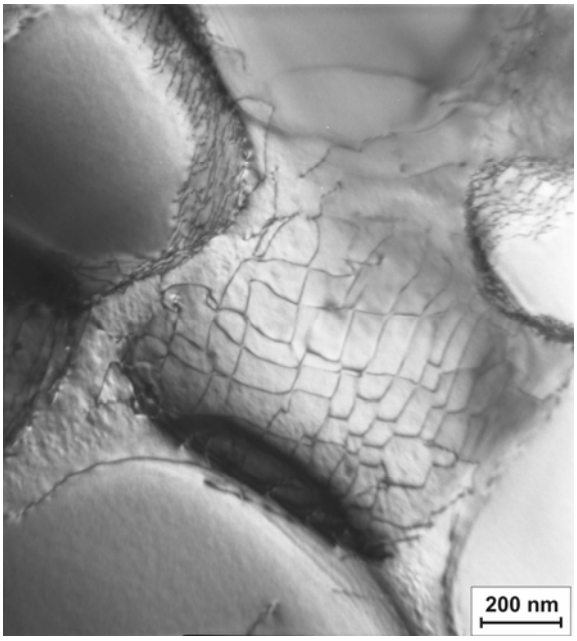

Fig. 8: Transmission electron micrograph showing an example of an interfacial dislocation network in Alloy Re

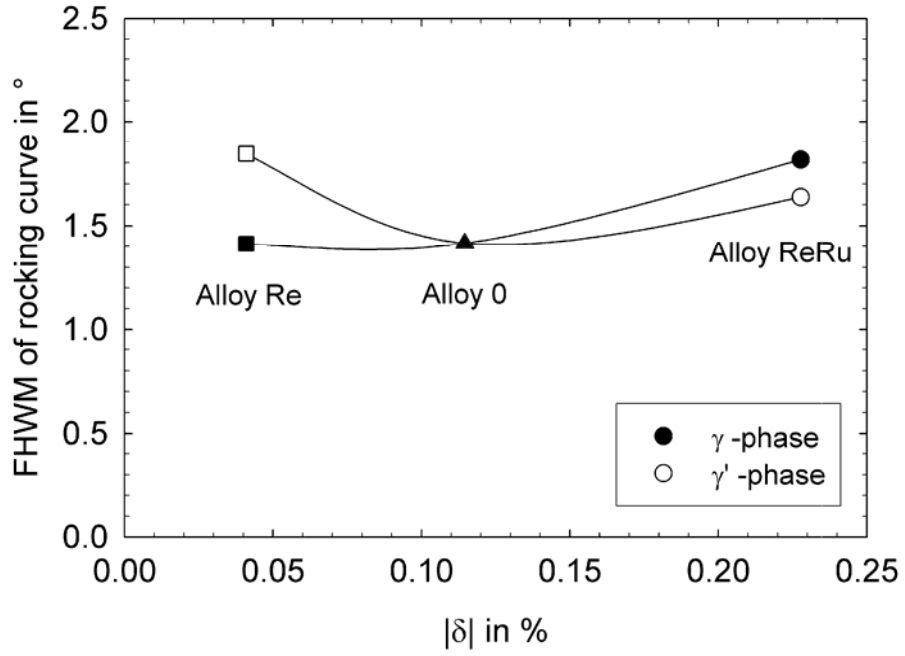

Fig. 9: Change of full width at half maximum of the rocking curves (ω-profiles) of the γ-phase (filled symbols) and γ′-phase (open symbols) of the investigated alloys after creep

Table 1: Nominal chemical composition and room temperature lattice constant of the γ- and γ′-phase of the experimental alloys investigated in this work

elements / wt-%	**Al**	**Ti**	**Cr**	**Co**	**Mo**	**Ta**	**Re**	**Ru**	**Ni**	**a(γ)**	**a(γ′)**
Alloy ReRu	4.9	3.9	8.2	4.1	2.5	1.6	**3.0**	**3.0**	68.8	0,35931	0,35849
Alloy Re	4.9	3.9	8.2	4.1	2.5	1.6	**3.0**	0	71.8	0,35826	0,35811
Alloy 0	4.9	3.9	8.2	4.1	2.5	1.6	0	0	74.8	0,35750	0,35791